10378 *Inorg. Chem.* **2010**, *49*, 10378–10389
DOI: 10.1021/ic101130m

Inorganic Chemistry
Article

Structural Study of the $Li_{0.5}Na_{0.5}MnFe_2(PO_4)_3$ and $Li_{0.75}Na_{0.25}MnFe_2(PO_4)_3$ Alluaudite Phases and Their Electrochemical Properties As Positive Electrodes in Lithium Batteries

Khiem Trad,[†,‡,§] Dany Carlier,*[,†,‡] Laurence Croguennec,[†,‡] Alain Wattiaux,[†] Mongi Ben Amara,[§] and Claude Delmas[†,‡]

[†]*CNRS, Université de Bordeaux, ICMCB, 87 avenue du Dr. A. Schweitzer, 33608 F-Pessac Cedex, France,* [‡]*CNRS, ENSCBP, ICMCB, 87 avenue du Dr. A. Schweitzer, 33608 F-Pessac Cedex, France, and* [§]*UR Matériaux Inorganiques, Faculté des Sciences de Monastir, avenue de l'environnement, 5019, Monastir, Tunisia*

Received June 4, 2010

The alluaudite lithiated phases $Li_{0.5}Na_{0.5}MnFe_2(PO_4)_3$ and $Li_{0.75}Na_{0.25}MnFe_2(PO_4)_3$ were prepared via a sol−gel synthesis, leading to powders with spongy characteristics. The Rietveld refinement of the X-ray and neutron diffraction data coupled with *ab initio* calculations allowed us for the first time to accurately localize the lithium ions in the alluaudite structure. Actually, the lithium ions are localized in the A(1) and A(1)′ sites of the tunnel. Mössbauer measurements showed the presence of some Fe^{2+} that decreased with increasing Li content. Neutron diffraction revealed the presence of a partial Mn/Fe exchange between the two transition metal sites that shows clearly that the oxidation state of the element is fixed by the type of occupied site. The electrochemical properties of the two phases were studied as positive electrodes in lithium batteries in the 4.5−1.5 V potential window, but they exhibit smaller electrochemical reversible capacity compared with the non-lithiated $NaMnFe_2(PO_4)_3$. The possibility of Na^+/Li^+ ion deintercalation from $(Na,Li)MnFe_2(PO_4)_3$ was also investigated by DFT+U calculations.

Introduction

The discovery of $LiFePO_4$'s behavior as a positive electrode in lithium batteries[1] enhanced the great interest for polyanion compounds as an alternative to oxides for lithium storage electrodes for rechargeable batteries such as $LiM(PO_4)$ (M = transition metals) with the olivine structure,[2,3] $A_xM'_2(XO_4)_3$ (A = Li, Na ; M′ = Ti, Fe, V and X = P, As)[4−6] with the Nasicon structure, $VOPO_4$,[7] $LiFe(P_2O_7)$[8] and $Fe_4(P_2O_7)_3$,[9] silicates,[10−12] and more recently $LiMPO_4(F,OH)$[13−15] and $LiMSO_4F$.[16] Since this class of compounds has low electronic conductivity, progress in overcoming their inherent insulating nature has been achieved by the formation of nanoparticles[17] and their intimate mixing with electronic conductive additives like carbon, metal, and metal oxide.[18−21] In the scope of

*To whom correspondence should be addressed. Phone: +33 (0) 5 40 00 31 75. Fax: +33 (0) 5 40 00 27 61. E-mail: carlier@icmcb-bordeaux.cnrs.fr.

(1) Padhi, A. K.; Nanjundaswamy, K. S.; Goodenough, J. B. *J. Electrochem. Soc.* **1997**, *144*, 1188–1194.
(2) Murugan, A. V.; Muraliganth, T.; Manthiram, A. *J. Electrochem. Soc.* **2009**, *156*, A79–A83.
(3) Kopeć, M.; Yamada, A.; Kobayashi, G.; Nishimura, S.; Kanno, R.; Mauger, A.; Gendron, F.; Julien, C. *J. Power Sources* **2009**, *189*, 1154–1163.
(4) Delmas, C.; Nadiri, A.; Soubeyroux, J. *Solid State Ionics* **1988**, *28−30*, 419–423. Proceedings of the 6th International Conference on Solid State Ionics.
(5) Masquelier, C.; Padhi, A. K.; Nanjundaswamy, K. S.; Goodenough, J. B. *J. Solid State Chem.* **1998**, *135*, 228–234.
(6) Patoux, S.; Wurm, C.; Morcrette, M.; Rousse, G.; Masquelier, C. *J. Power Sources* **2003**, *119−121*, 278–284. Selected papers presented at the 11th International Meeting on Lithium Batteries.
(7) Dupré, N.; Gaubicher, J.; Le Mercier, T.; Wallez, G.; Angenault, J.; Quarton, M. *Solid State Ionics* **2001**, *140*, 209–221.
(8) Ramana, C. V.; Ait-Salah, A.; Utsunomiya, S.; Mauger, A.; Gendron, F.; Julien, C. M. *Chem. Mater.* **2007**, *19*, 5319–5324.
(9) Masquelier, C.; Reale, P.; Wurm, C.; Morcrette, M.; Dupont, L.; Larcher, D. *J. Electrochem. Soc.* **2002**, *149*, A1037–A1044.
(10) Nytén, A.; Abouimrane, A.; Armand, M.; Gustafsson, T.; Thomas, J. O. *Electrochem. Commun.* **2005**, *7*, 156–160.
(11) Lyness, C.; Delobel, B.; Armstrong, A. R.; Bruce, P. G. *Chem. Commun.* **2007**, 4890–4892.
(12) Dominko, R. *J. Power Sources* **2008**, *184*, 462–468. Selected papers from the International Battery Materials Assocation 2007 Conference. In Memoriam of Juergen Besenhard.
(13) Ellis, B. L.; Makahnouk, W. R. M.; Makimura, Y.; Toghill, K.; Nazar, L. F. *Nat. Mater.* **2007**, *6*, 749–753.
(14) Recham, N.; Chotard, J.-N.; Jumas, J.-C.; Laffont, L.; Armand, M.; Tarascon, J.-M. *Chem. Mater.* **2010**, *22*, 1142–1148.
(15) Marx, N.; Croguennec, L.; Carlier, D.; Wattiaux, A.; Cras, F. L.; Suard, E.; Delmas, C. *Dalton Trans.* **2010**, *39*, 5108–5116.
(16) Recham, N.; Chotard, J.-N.; Dupont, L.; Delacourt, C.; Walker, W.; Armand, M.; Tarascon, J.-M. *Nat. Mater.* **2010**, *9*, 68–74.
(17) Yamada, A.; Chung, S. C.; Hinokuma, K. *J. Electrochem. Soc.* **2001**, *148*, A224–A229.
(18) Ravet, N.; Chouinard, Y.; Magnan, J. F.; Besner, S.; Gauthier, M.; Armand, M. *J. Power Sources* **2001**, *97−98*, 503–507.
(19) Huang, H.; Yin, S.-C.; Nazar, L. F. *Electrochem. Solid-State Lett.* **2001**, *4*, A170–A172.
(20) Croce, F.; Epifanio, A. D.; Hassoun, J.; Deptula, A.; Olczac, T.; Scrosati, B. *Electrochem. Solid-State Lett.* **2002**, *5*, A47–A50.
(21) Croce, F.; D'Epifanio, A.; Reale, P.; Settimi, L.; Scrosati, B. *J. Electrochem. Soc.* **2003**, *150*, A576–A581.

 Published on Web 10/15/2010

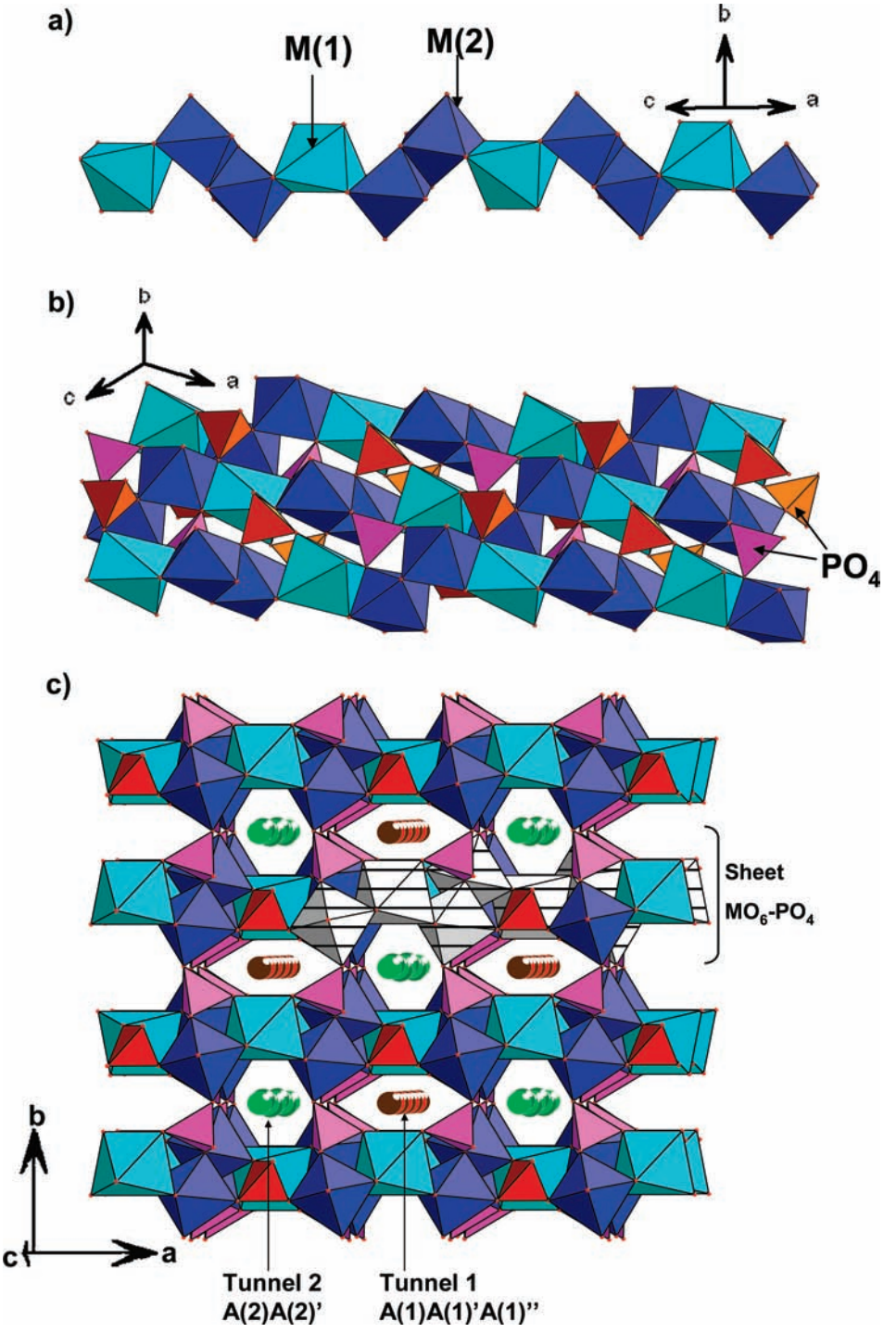

Figure 1. (a) View of the chain showing the distorted octahedral M(1) and M(2) sites. (b) View of the sheet constituted by MO_6 octahedra and PO_4 tetrahedra. (c) A perspective view of the alluaudite structure in the *ab* plane. The hatched polyhedra represent a chain.

searching for new positive electrode materials, we were recently interested in alluaudite $NaMnFe_2(PO_4)_3$ exhibiting the alluaudite structure. In a previous paper, we reported the optimized synthesis of this compound together with its structural characterization and electrochemical performance as a positive electrode in sodium and lithium cells.[22] We showed that the cycling performance is strongly dependent on the aggregate/particle morphology: Li^+ ions and electrons/f.u. could be intercalated in the material prepared by the sol−gel route. In this paper, we applied a similar synthesis method to prepare lithium substituted phases, i.e., $Li_{0.5}Na_{0.5}Mn^{II}Fe^{III}_2(PO_4)_3$ and $Li_{0.75}Na_{0.25}Mn^{II}Fe^{III}_2(PO_4)_3$, previously reported by Hatert et al.,[23] that also exhibit the alluaudite structure. The structure of these phases consists of chains formed by a succession of M(2) octahedral pairs linked by highly distorted M(1) octahedra (Figure 1a). Equivalent chains are

(22) Trad, K.; Carlier, D.; Croguennec, L.; Wattiaux, A.; Lajmi, B.; Ben Amara, M.; Delmas, C. Submitted to *Chem. Mater*.

(23) Hatert, F.; Keller, P.; Lissner, F.; Antenucci, D.; Fransolet, A.-M. *Eur. J. Mineral.* **2000**, *12*, 847–857.

Table 1. Chemical Analysis Results and Lattice Parameters Obtained from le Bail Method Refinement of the XRD Data of the $Li_yNa_{1-y}MnFe_2(PO_4)_3$ (with $y = 0, 0.5, 0.75$) Compounds (All Crystallize in the $C2/c$ Monoclinic Space Group)

theoretical compositions	$NaMnFe_2(PO_4)_3$	$Li_{0.5}Na_{0.5}MnFe_2(PO_4)_3$	$Li_{0.75}Na_{0.25}MnFe_2(PO_4)_3$
experimental compositions	$Na_{0.95(5)}Mn_{1.09(5)}Fe_{2.02(5)}(PO_4)_3$ [22]	$Li_{0.51(5)}Na_{0.50(5)}Mn_{1.08(5)}Fe_{2.10(5)}(PO_4)_3$	$Li_{0.77(5)}Na_{0.25(5)}Mn_{1.09(5)}Fe_{2.05(5)}(PO_4)_3$
a (Å)	11.9878(2)	11.9892(2)	11.9822(2)
b (Å)	12.5364(2)	12.4927(2)	12.4672(1)
c (Å)	6.3980(1)	6.3859(1)	6.3787(1)
β (deg)	114.220(1)	114.639(1)	114.800(6)
V (Å^3)	876.88(4)	869.39(4)	865.01(3)
		Conditions of the X-Ray Diffraction Experiments	
wavelength		1.5405 Å	
temperature		293 K	
angular range		$5° \le 2\theta \le 120°$	
step scan increment (2θ)		0.0167°	
sample displacement (2θ)		0.02(1)°	
profile parameters:		$\eta = 0.6(1)$	$\eta = 0.17(4)$
pseudo-Voigt function		$U = 0.1(1)$	$U = 0.04(2)$
		$V = -0.001(2)$	$V = -0.003(1)$
		$W = 0.004(2)$	$W = 0.005(1)$
conventional Rietveld R factors		$R_{wp} = 18.2\%$; $R_B = 18\%$; Scor = 2.1	$R_{wp} = 13.8\%$; $R_B = 14\%$; Scor = 2.2

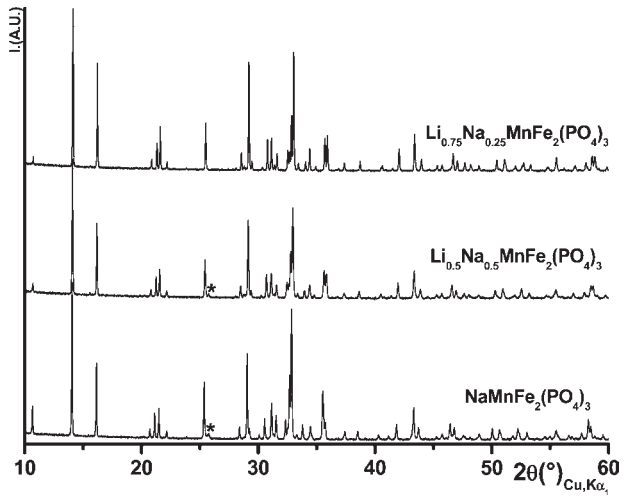

Figure 2. Comparison of the XRD patterns of $Li_yNa_{1-y}MnFe_2(PO_4)_3$ (with $y = 0$, 0.5, and 0.75).

connected by phosphate tetrahedra to form sheets extended in the (a,c) plane of the monoclinic cell (Figure 1b). Equivalent sheets are held together by PO_4 tetrahedra to form a three-dimensional architecture with two sets of tunnels in the c direction thus formed: tunnel 1 (1/2, 0, z) and tunnel 2 (0, 0, z) (Figure 1c). Richardson reported a preliminary study of some other alluaudite compounds, $Li_{0.75}Na_{0.25}MnFe_2(PO_4)_3$, $Na_2FeMn_2(PO_4)_3$, and $LiNaFeMn_2(PO_4)_3$, that exhibit poor electrochemical activity in lithium batteries.[24]

In this paper, we report the synthesis of $Li_{0.5}Na_{0.5}MnFe_2(PO_4)_3$ and $Li_{0.75}Na_{0.25}MnFe_2(PO_4)_3$ phases and their structural study by X-ray and neutron diffraction techniques and Mössbauer spectroscopy, supported by *ab initio* calculations. Finally, we studied their electrochemical behavior in lithium cells in comparison with those of $NaMnFe_2(PO_4)_3$.

Experimental Section

$Li_yNa_{1-y}MnFe_2(PO_4)_3$ ($0 \le y \le 1$) compounds were synthesized via a sol−gel preparation route.[22] Stoichiometric amounts of Na_2CO_3 (pure, Riedel-de Haën), Li_2CO_3 (99%, Alfa Aesar), $MnCO_3$ (99.9%, Aldrich), $FeC_2O_4 \cdot 2H_2O$ (pure, Prolabo), and $(NH_4)H_2PO_4$ (98.5%, Sigma Aldrich) were mixed in distilled water with sufficient nitric acid added to total dissolution, in which citric acid was also added as a complexing agent for the formation of the gel. The molar ratio of citric acid to total metal ions was equal to unity. The solutions were heated under vigorous stirring until the water evaporated, leading to the formation of a viscous gel. The as-formed gel was further heated until decomposition of the organic compounds; a spontaneous exothermic decomposition reaction occurred, resulting in the formation of a voluminous black, fine powder. The decomposed precursors were ground and introduced in a furnace and preheated at 800 °C for 30 min under an air atmosphere. Green fine powders were obtained by quenching the products in the air.

The particle morphology was characterized by scanning electron microscopy (SEM) using a Hitachi S-450 emission field microscope. The powders were metallized by gold−palladium plasma.

The phase composition was carefully controlled by quantitative analysis employing inductively coupled plasma (ICP) to determine the Na/P, Li/P, Mn/P, and Fe/P ratios using an ICP-OES (Varian 720-ES Optical Emission Spectrometer) plasma emission spectrometer with an argon flow for the plasma.

The X-ray diffraction patterns were collected using a PANalytical X'pert Pro diffractometer (Cu Kα1 radiation, antiscatter slit of 1/2° and divergence slit of 1° on the incident beam path). The diffraction patterns were recorded in the 5−120° (2θ) angular range using a 0.0167° (2θ) step and a constant counting time of 10 s. Neutron diffraction data were recorded on the D2B high resolution powder diffractometer of Institut Laue Langevin (ILL) at Grenoble (France) in the transmission mode with a 1.595 Å wavelength. The diffraction patterns were collected at ambient temperature from 0 to 160° (2θ) with a 0.05° step and a total counting time of 4 h. The X-ray and neutron diffraction patterns were analyzed using the Fullprof program. In order to take the sample radiation absorption into account during the structural refinement of the neutron data, a corrective term μR equal to 0.162 for $Li_{0.5}Na_{0.5}MnFe_2(PO_4)_3$ and 0.162 for $Li_{0.75}Na_{0.25}MnFe_2(PO_4)_3$ was used, where μ is the absorption coefficient and R is the radius of the vanadium cylinder sample container. μ is defined as $\mu = {}^{n}/_{V}\sum_i n_i\sigma_i$, where n is the number of units in the unit cell, V is the cell volume, n_i is the number of a given atom in the formula unit, and σ_i is the sum of coherent and incoherent scattering cross sections for atom i.

Mössbauer spectra were recorded in transmission mode at room temperature on a constant-acceleration spectrometer

(24) Richardson, T. J. *J. Power Sources* **2003**, *119−121*, 262–265.

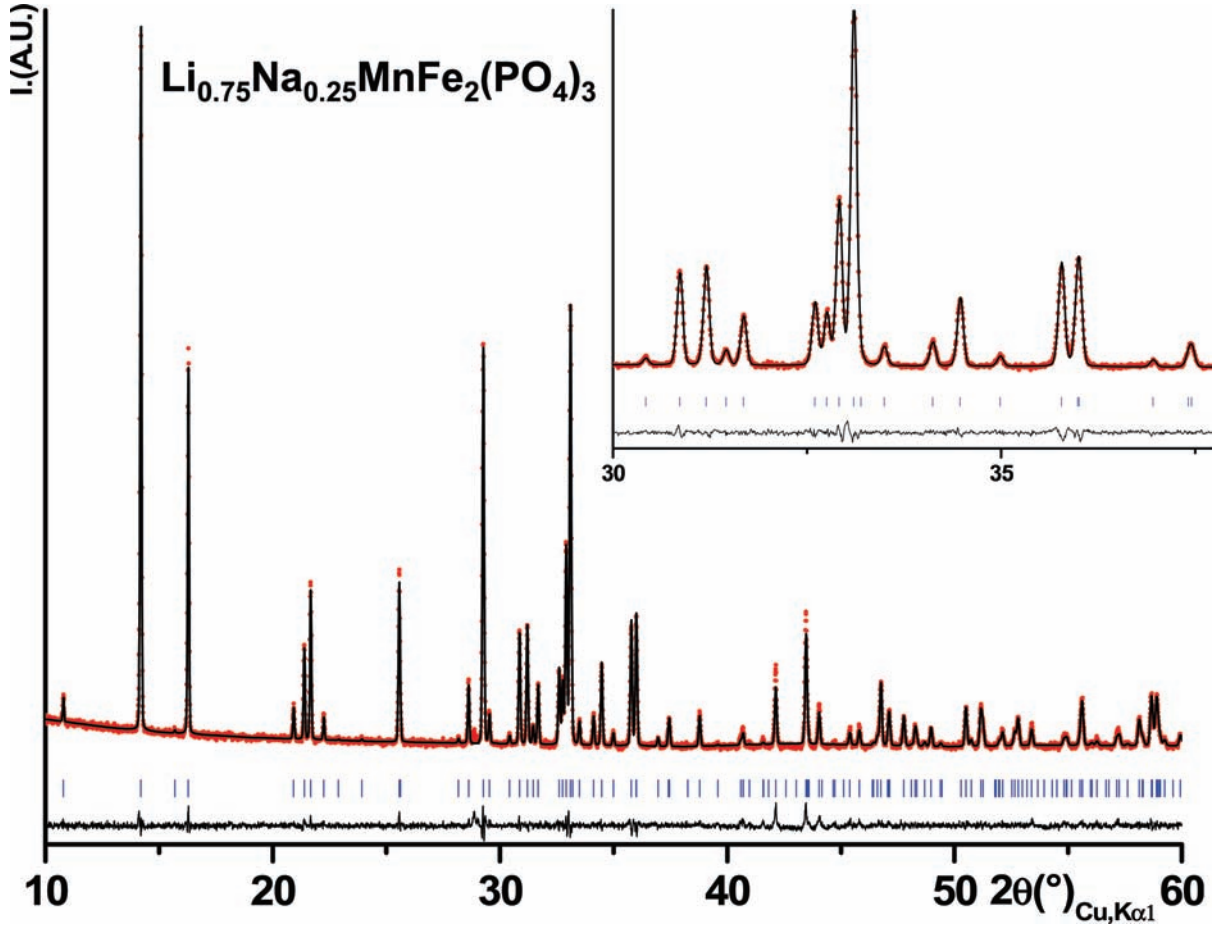

Figure 3. Comparison of the experimental and calculated X-ray diffraction patterns of $Li_{0.75}Na_{0.25}MnFe_2(PO_4)_3$. Enlargement of the plot in the 30−37.5° (2θ) range is given in the inset.

using a ^{57}Co/Rh source. The velocity scale and the origin of the isomer shift were calibrated using the spectrum of a high-purity α-Fe foil. All of the spectra were recorded in a large range of velocities (−10 mm/s; +10 mm/s) and have shown the absence of magnetic impurities in the sample and especially of α-Fe_2O_3, which is magnetic at room temperature. The refined hyperfine interaction parameters were isomeric shift (δ), quadrupole splitting (Δ), resonance line width (Γ), and relative fraction of the spectral components. The latter was determined assuming an equal recoil-free factor (f) for each of the ^{57}Fe nuclei in the structure.

First-principles calculations were performed using density functional theory (DFT) in the generalized gradient approximation (GGA; PBE)[25] and GGA+U with the projector augmented wave (PAW) method,[26] as implemented in the Vienna Ab Initio Simulation Package (VASP).[27] A plane wave cutoff energy of 500 eV and a 2 × 2 × 2 k-point grid were used for all cells in order to get the total energy to be converged by less than 5 meV/unit cell. The structures were relaxed, and the final energies of each optimized geometry were recalculated so as to correct for the changes in basis during relaxation. Previous studies showed that the GGA method allows a better simulation of magnetic interactions and Jahn−Teller distortions than the LDA method.[28] The DFT+U method allows a more accurate treatment of the electronic structure of strongly correlated systems and was shown to be particularly adapted to treat the transition metal phosphates and recover the experimental average voltages.[29] In our study, Dudarev's approach was used in order to perform the GGA+U. In this method, the parameters U ("on site" electron−electron repulsion) and J (exchange interaction) are not entered separately, as only the difference ($U - J$) is meaningful. It, therefore, allows the specification of a single parameter that will be called $U_{eff} = U - J$. Recently, Zhou et al. developed a method to evaluate the U value *ab initio*[29] for a given exchange J value. In our study, we therefore used the U_{eff} values determined for high-spin Fe^{3+} and Mn^{2+} ions in the olivine MPO_4,[29] i.e., $U_{eff} = 4.9$ eV for high-spin Fe^{3+} and $U_{eff} = 3.92$ eV for high-spin Mn^{2+}. As our magnetic measurements (not shown here) did not reveal any magnetic transition at low temperatures, calculations were performed in the ferromagnetic configuration.

Electrochemical studies were carried out in lithium coin cells, prepared in a glovebox under an argon atmosphere. The positive electrodes consisted of $Li_yNa_{1-y}MnFe_2(PO_4)_3$ (y = 0.5, 0.75) powders which were first ball-milled with carbon black for 15 min; this mixture was then added to polyvinylidene fluoride with a weight ratio of 80:15:5. Some drops of N-methyl pyrrolidone (NMP) were added to get a fluid mixture. The resulting slurry was spread uniformly onto an aluminum foil, which was pressed, cut into disks, and then dried under vacuum conditions at 100 °C overnight. Metallic lithium was used as the negative electrode with 1 M $LiPF_6$ in a

(25) Perdew, J. P.; Burke, K.; Ernzerhof, M. *Phys. Rev. Lett.* **1996**, *77*, 3865.
(26) Kresse, G.; Joubert, D. *Phys. Rev. B* **1999**, *59*, 1758.
(27) Kresse, G.; Furthmüller, J. *Phys. Rev. B* **1996**, *54*, 11169.
(28) Mishra, S. K.; Ceder, G. *Phys. Rev. B* **1999**, *59*, 6120.
(29) Zhou, F.; Cococcioni, M.; Marianetti, C. A.; Morgan, D.; Ceder, G. *Phys. Rev. B* **2004**, *70*, 235121.

mixture of propylene carbonate (PC), ethylene carbonate (EC), and dimethyl carbonate (DMC) (1:1:3) as the electrolyte. The electrochemical tests were carried out in the galvanostatic mode with a homemade apparatus or with a Biologic VMP1 system.

Results and Discussions

An X-ray diffraction study has shown that all of the $Li_yNa_{1-y}MnFe_2(PO_4)_3$ compounds with $y < 0.8$ and prepared by the sol−gel method as described in the Experimental Section exhibit the alluaudite structure. Syntheses performed for $y \geq 0.8$ lead to a mixture of an alluaudite phase with a significant amount of $Li_3Fe_2(PO_4)_3$ as an impurity. In this paper, we chose to focus on the $y = 0.5$ and 0.75 compositions in comparison with the nonsubstituted $NaMnFe_2(PO_4)_3$ phase. ICP measurements confirmed the expected chemical compositions of the synthesized phases (Table 1). The XRD patterns of $Li_yNa_{1-y}MnFe_2(PO_4)_3$ ($y = 0$, 0.5, 0.75) are given in Figure 2. The phases exhibit diffraction lines expected for the alluaudite structure crystallizing in the monoclinic $C2/c$ space group. Note that the XRD patterns of the phases synthesized with $y = 0$ and $y = 0.5$ exhibit the major diffraction line of quartz α-$FePO_4$ (indicated by ∗ in Figure 2). In the following, in agreement with the result of the chemical analyses and the negligible amount of quartz α-$FePO_4$, the formulas of the studied materials are considered to be the nominal ones. The XRD patterns of the $Li_yNa_{1-y}MnFe_2(PO_4)_3$ ($y = 0$, 0.5, 0.75) phases were first analyzed using the Le Bail method:[30] only the unit cell parameters and the profile parameters of a pseudo-Voigt function were refined. As given in Table 1, the b and c lattice parameters and the unit cell volume show a regular decrease (almost linear) with increasing the lithium amount (y), while the β angle increases. These observations can be expected from the ionic radius difference between Li^+ ($r = 0.74$ Å) and Na^+ ($r = 1.02$ Å). The lattice parameters are slightly different from those reported in the literature for $Li_{0.5}Na_{0.5}MnFe_2(PO_4)_3$ [$a = 12.988(2)$ Å, $b = 12.500(3)$ Å, $c = 6.392(1)$ Å, and $\beta = 114.67(3)°$][23] and for $Li_{0.75}Na_{0.25}MnFe_2(PO_4)_3$ [$a = 11.976(4)$ Å, $b = 12.467(3)$ Å, $c = 6.388(2)$ Å, and $\beta = 114.86(2)°$].[23] As their synthesis procedure differs from ours, the cationic distribution might differ, as discussed in the following.

The full structural refinement of the X-ray and neutron diffraction patterns is reported elsewhere for the nonsubstituted $NaMnFe_2(PO_4)_3$ phase.[22] In that case, neutron diffraction was performed in order to distinguish iron and manganese ions that exhibit similar X-ray scattering factors but very different (in magnitude and sign) Fermi lengths (b(Fe) = 0.945×10^{-12} cm and b(Mn) = -0.373×10^{-12} cm). We evidenced an Fe/Mn exchange between the M(1) and M(2) sites that is associated with a change in the oxidation state of iron and manganese. The following formula was thus proposed for $NaMnFe_2(PO_4)_3$: $(Na_{0.81})_{A(1)}(Na_{0.19})_{A(2)'}(Mn^{II}_{0.87}Fe^{II}_{0.13})_{M(1)}(Fe^{III}_{1.87}Mn^{III}_{0.13})_{M(2)}(PO_4)_3$. Applying the same strategy, we report here the structural study of the $Li_{0.5}Na_{0.5}MnFe_2(PO_4)_3$ and $Li_{0.75}Na_{0.25}MnFe_2(PO_4)_3$ phases on the basis of the X-ray and neutron diffraction pattern analysis. In the present study, neutron diffraction will provide additional information concerning the lithium ion sites (the Li scattering factor being much greater for neutron diffraction (b(Li) = -0.19×10^{-12} cm) than for X-ray diffraction).

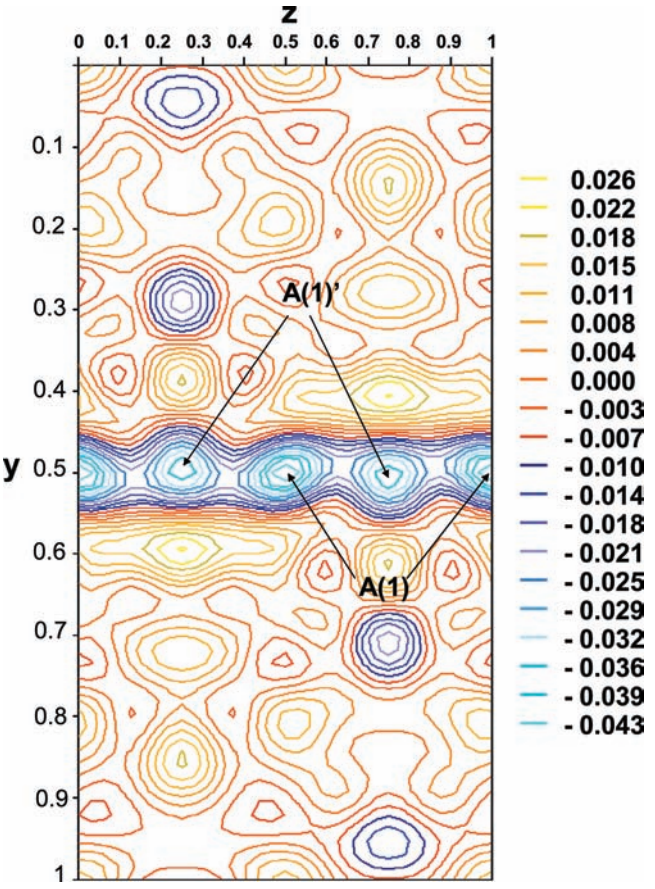

Figure 4. Fourier difference map showing the residual nuclear density in the (b,c) plane considering only Na, Mn, Fe, P, and O ions in the structural model.

For the Rietveld refinement, the total amount of alkaline ions in the structure was constrained to one, and the M(1) and M(2) sites were respectively constrained to full occupancy. We first localized, by analyzing the XRD data, the sodium ion in $Li_{0.5}Na_{0.5}MnFe_2(PO_4)_3$ and $Li_{0.75}Na_{0.25}MnFe_2(PO_4)_3$ by calculating Fourier difference maps considering the Mn and Fe transition metal ions in the M(1) and M(2) sites. For the two lithiated compounds, and in agreement with the literature,[23] sodium ions were shown to partially occupy the A(1) and A(2)′ sites located respectively in tunnels 1 and 2 of the structure, similarly to what is observed for the $NaMnFe_2(PO_4)_3$ phase, but with different occupation ratios as it will be discussed in details in the following. Figure 3 shows the comparison between the experimental and calculated XRD patterns of $Li_{0.75}Na_{0.25}MnFe_2(PO_4)_3$; the good minimization of the difference reveals the good description of the structure by the model considered (even if still incomplete at this step).

The Rietveld refinements of the neutron diffraction data were then carried out in a similar manner to the $NaMnFe_2(PO_4)_3$ phase: manganese and iron ions were mainly located respectively in the M(1) and M(2) sites with an Fe/Mn site exchange; then their atomic positions and occupancies were refined. The amount of exchanged ions, however, decreases when the amount of lithium in substitution of sodium increases: we found 0.13 for $NaMnFe_2(PO_4)_3$,[22] ∼0.08 for $Li_{0.5}Na_{0.5}MnFe_2(PO_4)_3$, and ∼0.04 for $Li_{0.75}Na_{0.25}MnFe_2(PO_4)_3$.

(30) Bail, A. L.; Duroy, H.; Fourquet, J. *Mater. Res. Bull.* **1988**, *23*, 447–452.

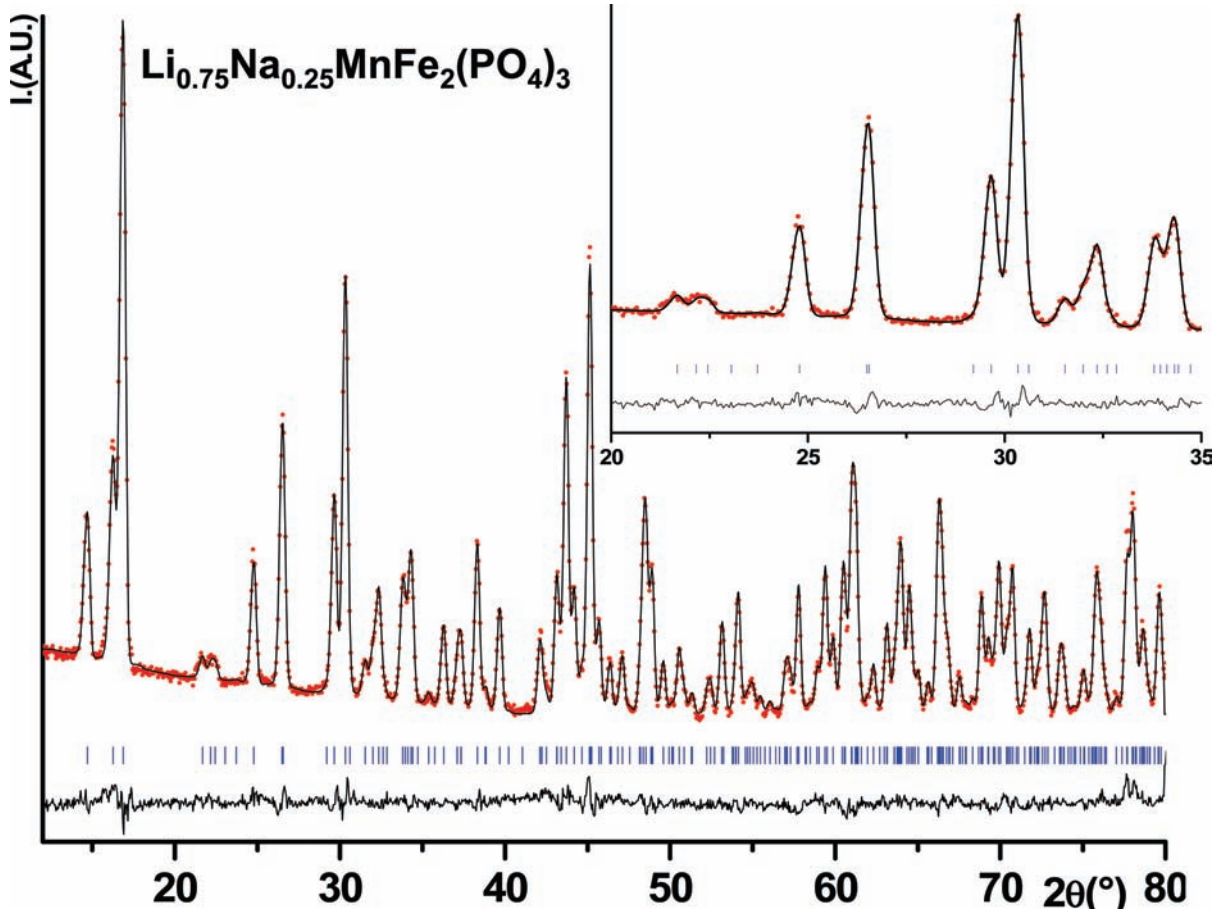

Figure 5. Comparison of the experimental and calculated neutron diffraction patterns of $Li_{0.75}Na_{0.25}MnFe_2(PO_4)_3$. Enlargement of the plot in the range 20−35° (2θ) is given in the inset.

Table 2. Profile and Structural Parameters Obtained after Full Rietveld Refinement of the Experimental Neutron Diffraction Patterns of $Li_yNa_{1-y}MnFe_2(PO_4)_3$ (with y = 0.5, 0.75)[a]

		$NaMnFe_2(PO_4)_3$[22]				$Li_{0.5}Na_{0.5}MnFe_2(PO_4)_3$				$Li_{0.75}Na_{0.25}MnFe_2(PO_4)_3$			
		x	*y*	*z*	occ.	*x*	*y*	*z*	occ.	*x*	*y*	*z*	occ.
Li(1)	A(1) 4b					1/2	0	0	0.294(2)	1/2	0	0	0.309(2)
Li(2)	A(1)′4e					0	0.501(8)	1/4	0.206(2)	0	0.501(7)	1/4	0.441(2)
Na(1)	A(1) 4b	1/2	0	0	0.815(1)	1/2	0	0	0.289(1)	1/2	0	0	0.086(1)
Na(2)	A(2)′4e	0	0.022(6)	1/4	0.185(1)	0	0.014(1)	1/4	0.211(1)	0	0.011(1)	1/4	0.164(1)
Mn(1)	M(1)4e	0	0.261(2)	1/4	0.870(3)	0	0.262(1)	1/4	0.926(1)	0	0.261(8)	1/4	0.958(1)
Fe(2)	M(1)4e	0	0.261(6)	1/4	0.130(3)	0	0.262(1)	1/4	0.074(1)	0	0.261(8)	1/4	0.042(1)
Fe(1)	M(2) 8f	0.219(3)	0.151(3)	0.129(7)	0.935(3)	0.220(2)	0.153(2)	0.131(6)	0.963(1)	0.219(2)	0.152(2)	0.129(5)	0.979(1)
Mn(2)	M(2) 8f	0.219(3)	0.151(3)	0.129(7)	0.065(3)	0.220(2)	0.153(2)	0.131(6)	0.037(1)	0.219(2)	0.152(2)	0.129(5)	0.021(1)
P(1)	4e	0	−0.285(6)	1/4	1	0	−0.286(6)	1/4	1	0	−0.287(5)	1/4	1
P(2)	8f	0.242(5)	−0.108(6)	0.130(1)	1	0.241(5)	−0.108(4)	0.128(9)	1	0.242(4)	−0.108(4)	0.133(8)	1
O(1)	8f	0.454(5)	0.714(5)	0.532(2)	1	0.453(4)	0.715(3)	0.532(8)	1	0.452(3)	0.716(3)	0.530(7)	1
O(2)	8f	0.098(5)	0.640(8)	0.241(2)	1	0.099(3)	0.638(3)	0.237(7)	1	0.099(3)	0.636(3)	0.238(7)	1
O(3)	8f	0.329(5)	0.663(5)	0.103(1)	1	0.327(4)	0.663(3)	0.103(8)	1	0.327(4)	0.665(3)	0.101(7)	1
O(4)	8f	0.119(5)	0.396(4)	0.311(1)	1	0.120(4)	0.399(3)	0.305(8)	1	0.120(4)	0.399(3)	0.305(7)	1
O(5)	8f	0.224(5)	0.822(4)	0.316(1)	1	0.226(4)	0.822(3)	0.320(7)	1	0.223(3)	0.823(3)	0.320(6)	1
O(6)	8f	0.312(5)	0.502(3)	0.374(1)	1	0.314(4)	0.501(4)	0.375(8)	1	0.314(3)	0.504(4)	0.374(7)	1
						conditions of the neutron run							
wavelength						1.5955(8) Å							
temperature						293 K							
angular range						0° ≤ 2θ ≤ 160°							
step scan increment (2θ)						0.05°							
profile parameters:						η = 0.59(2)				η = 0.15(1)			
pseudo-Voigt function						U = 0.4(2)				U = 0.27(2)			
						V = −0.37(2)				V = −0.33(2)			
						W = 0.21(1)				W = 0.2(04)			
conventional Rietveld R factors						R_{wp} = 8.3%; R_B = 3.6%; Scor = 1.9				R_{wp} = 7.8%; R_B = 4.1%; Scor = 2.5			

[a] For comparison structural parameters of $NaMnFe_2(PO_4)_3$ are given.[22]

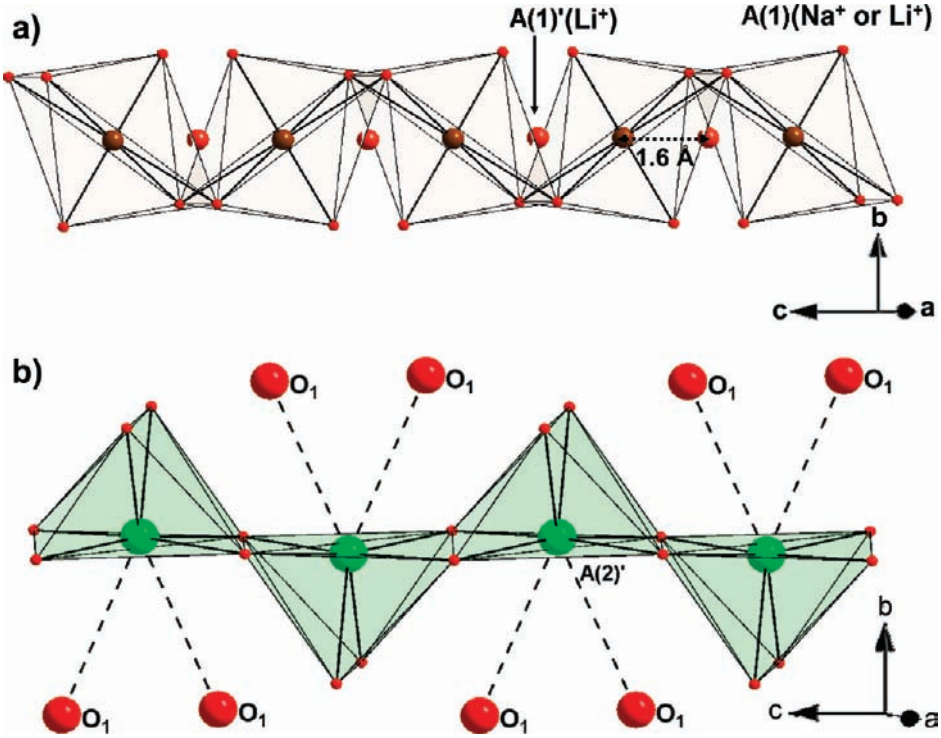

Figure 6. Local environments of the A(1) and A(1)′ (a) and A(2)′ (b) crystallographic sites determined from the Rietveld analysis of the X-ray and neutron diffraction data. The dotted bonds in b are too long to be considered in the Na(2) site.

Table 3. Selected Interatomic M−O and P−O Distances (Å) Determined for $Li_yNa_{1-y}MnFe_2(PO_4)_3$ (with $x = 0.5, 0.75$) from the Rietveld Refinement of the Neutron Diffraction Data

$Li_{0.5}Na_{0.5}MnFe_2(PO_4)_3$	$Li_{0.75}Na_{0.25}MnFe_2(PO_4)_3$
M(1)−O(1) = 2.1(1) Å × 2	M(1)−O(1) = 2.16(1) Å × 2
M(1)−O(3) = 2.24(1) Å × 2	M(1)−O(3) = 2.27(1) Å × 2
M(1)−O(4) = 2.17(1) Å × 2	M(1)−O(4) = 2.16(1) Å × 2
⟨M(1)−O⟩ = 2.2 Å	⟨M(1)−O⟩ = 2.2 Å
$\Delta M(1) = 2.5 \times 10^{-4}$	$\Delta M(1) = 5.3 \times 10^{-4}$
M(2)−O(1) = 2.05(1) Å	M(2)−O(1) = 2.05(1) Å
M(2)−O(2) = 1.96(1) Å	M(2)−O(2) = 1.99(1) Å
M(2)−O(3) = 2.01(1) Å	M(2)−O(3) = 2.01(1) Å
M(2)−O(5) = 2.03(2) Å	M(2)−O(5) = 2.05(1) Å
M(2)−O(5) = 2.18(1) Å	M(2)−O(5) = 2.22(1) Å
M(2)−O(6) = 1.93(1) Å	M(2)−O(6) = 1.91(1) Å
⟨M(2)−O⟩ = 2.03 Å	⟨M(2)−O⟩ = 2.04 Å
$\Delta M(2) = 6.3 \times 10^{-3}$	$\Delta M(2) = 2.0 \times 10^{-3}$
P(1)−O(1) = 1.53(1) Å × 2	P(1)−O(1) = 1.54(1) Å × 2
P(1)−O(2) = 1.54(1) Å × 2	P(1)−O(2) = 1.55(1) Å × 2
⟨P(1)−O⟩ = 1.54 Å	⟨P(1)−O⟩ = 1.55 Å
$\Delta P(1) = 8.6 \times 10^{-6}$	$\Delta P(1) = 3.4 \times 10^{-5}$
P(2)−O(3) = 1.52(1) Å	P(2)−O(3) = 1.53(1) Å
P(2)−O(4) = 1.52(1) Å	P(2)−O(4) = 1.55(1) Å
P(2)−O(5) = 1.57(1) Å	P(2)−O(5) = 1.53(1) Å
P(2)−O(6) = 1.52(1) Å	P(2)−O(6) = 1.52(1) Å
⟨P(2)−O⟩ = 1.53 Å	⟨P(2)−O⟩ = 1.53 Å
$\Delta P(2) = 2.0 \times 10^{-4}$	$\Delta P(2) = 7.1 \times 10^{-5}$

Then, to locate the lithium ions, the previous refinement results were input to the Rietveld refinement of the neutron data and after that Fourier difference maps were calculated. Figure 4 shows the Fourier difference map obtained in the case of lithium localization in the $Li_{0.5}Na_{0.5}MnFe_2(PO_4)_3$ structure. Residual densities were found not only in the 4*b* (1/2, 0, 0) position, which corresponds to the A(1) site, but also in the 4*e* (0, ∼1/2, 1/4) position, which was identified as the A(1)′ site in the tunnel 1.[31,23] The same results were obtained for lithium localization in the $Li_{0.75}Na_{0.25}MnFe_2(PO_4)_3$ structure. The site occupancies were refined by considering their sum to be equal to 0.5 and 0.75, respectively, for each lithiated phase. In $Li_{0.5}Na_{0.5}MnFe_2(PO_4)_3$, the lithium ions are located preferentially in the A(1) site [0.29(1) Li^+ in A(1) and 0.21(1) Li^+ in A(1)′], whereas in $Li_{0.75}Na_{0.25}MnFe_2(PO_4)_3$, the lithium ions occupy preferentially the A(1)′ site [0.31(2) A(1) and 0.44(2) in A(1)′]. Figure 5 shows for $Li_{0.75}Na_{0.25}MnFe_2(PO_4)_3$ the resulting calculated neutron diffraction pattern in comparison with the experimental one. The good minimization of the difference ($I_{obs.} - I_{calc.}$) confirms the adequacy of the considered structural model to describe the lithiated alluaudite structure. The results obtained for the phases $Li_yNa_{1-y}MnFe_2(PO_4)_3$ ($y = 0.5$ and 0.75) by the Rietveld refinement of their neutron diffraction data are gathered in Table 2, in comparison with those of $NaMnFe_2(PO_4)_3$. The corresponding M−O and P−O distances are given in Table 3, and the Na−O and Li−O distances are given in Table 4.

Table 4. Selected Interatomic A−O Distances (Å) Determined for $Li_yNa_{1-y}MnFe_2(PO_4)_3$ (with $x = 0.5, 0.75$) from the Rietveld Refinement of the Neutron Diffraction Data

$Li_{0.5}Na_{0.5}MnFe_2(PO_4)_3$	$Li_{0.75}Na_{0.25}MnFe_2(PO_4)_3$
A(1) = Na or Li	A(1) = Na or Li
A(1)−O(2) = 2.28(1) Å × 2	A(1)−O(2) = 2.22(1)Å × 2
A(1)−O(4) = 2.26(1) Å × 2	A(1)−O(4) = 2.20(1) Å × 2
A(1)−O(4) = 2.60(1) Å × 2	A(1)−O(4) = 2.55(1) Å × 2
A(1)′ = Li	A(1)′ = Li
A(1)′−O(2) = 2.10(1) Å × 2	A(1)′−O(2) = 2.04(6) Å × 2
A(1)′−O(4) = 1.84(1) Å × 2	A(1)′−O(4) = 1.81(5) Å × 2
A(2)′ = Na	A(2)′ = Na
A(2)′−O(3) = 2.65(1) Å × 2	A(2)′−O(3) = 2.84(3) Å × 2
A(2)′−O(6) = 2.50(1) Å × 2	A(2)′−O(6) = 2.452(3) Å × 2
A(2)′−O(6) = 2.66(1) Å × 2	A(2)′−O(6) = 2.654(5) Å × 2
A(2)′−O(1) = 3.13(1) Å × 2	A(2)′−O(1) = 2.94(3) Å × 2

(31) Warner, T. E.; Milius, W.; Maier, J. *J. Solid State Chem.* **1993**, *106*, 301–309.

The Na^+ and Li^+ Sites. According to the Rietveld refinement results for both $Li_{0.5}Na_{0.5}MnFe_2(PO_4)_3$ and $Li_{0.75}Na_{0.25}MnFe_2(PO_4)_3$ compounds, the sodium ions are located in A(1) and A(2)′ sites, in agreement with the results that we obtained for $NaMnFe_2(PO_4)_3$[22] and with other reports in the literature.[32−36] In the $NaMnFe_2(PO_4)_3$ compound, the Na^+ ions were distributed in the A(1) and the A(2)′ sites with a predominance in the A(1) site that was shown to be the most stable one by first principles calculations.[22] As sodium is substituted by lithium, the amount of sodium ions in the A(1) site decreases significantly, but the amount of Na^+ ions in the A(2)′ sites remains approximately constant: between 0.17 and 0.21 Na^+ ions are always present in tunnel 2. As illustrated in Figure 6a, the A(1) site is a distorted octahedral site. The A(2)′ site, as seen in Figure 6b, is a distorted prismatic site (see Table 2 for the six bond lengths). Note that two other oxygen ions are located at distances larger than 2.94 Å and were not considered here in the coordination polyhedra (shown by dotted bonds in Figure 6b).

In their crystallographic studies by XRD of lithiated alluaudite phases, Hatert and co-workers considered that the lithium ions were partially located exclusively in the A(1) and A(2)′ sites.[23,37,33,38,39] In our study, neutron diffraction allowed us to determine unambiguously the Li positions in the $Li_{0.5}Na_{0.5}MnFe_2(PO_4)_3$ and in $Li_{0.75}Na_{0.25}MnFe_2(PO_4)_3$ phases; i.e., in both phases, the lithium ions are located in A(1) and A(1)′ sites of tunnel 1. However, the lithium ions are preferentially located in the A(1) site in $Li_{0.5}Na_{0.5}MnFe_2(PO_4)_3$ and in the A(1)′ sites in $Li_{0.75}Na_{0.25}MnFe_2(PO_4)_3$. The A(1)′ site, represented in Figure 6a, consists of a very flat tetrahedral site, which is unusual for lithium ions but has already been seen in others phosphates.[40]

In order to investigate the lithium site stability and interpret the change in the predominant lithium site from $Li_{0.5}Na_{0.5}MnFe_2(PO_4)_3$ to $Li_{0.75}Na_{0.25}MnFe_2(PO_4)_3$, we performed theoretical calculations using the GGA and the GGA+U methods. The same methods were used to investigate the sodium sites' stability in $NaMnFe_2(PO_4)_3$,[22] and the results are also given in Figure 7a for comparison with the lithium case. The structural model considered for these calculations was the "ideal" one, i.e., $AMnFe_2(PO_4)_3$ (A = Na or Li) with no Mn/Fe site exchange. In the calculations, the alkaline ion was considered to fully occupy each of the A sites reported by Hatert et al.:[23] A(1)(4b)(1/2,0,0), A(1)′(4e)(0,∼0.5,1/4), A(2)(4a)(0,0,0), and A(2)′(4e)(0,∼0,1/4). All structures were then fully relaxed. In both GGA and GGA+U calculations, the most stable structure found for $NaMnFe_2(PO_4)_3$ is obtained with Na^+ ions in the A(1) sites, whereas the most stable structure found for $LiMnFe_2(PO_4)_3$ is obtained with Li^+ ions in the A(1)′ sites. In Figure 7a, the energies obtained for various alkaline distributions are represented by their differences from the reference energies and are expressed per $AMnFe_2(PO_4)_3$ formula unit. Despite some differences in the gaps between energies calculated with GGA or GGA+U methods, the relative site stability obtained with the two methods is the same: the two sites considered in tunnel 1, i.e., A(1) and A(1)′, are more stable than the two sites considered in tunnel 2, A(2) and A(2)′ for both $NaMnFe_2(PO_4)_3$ and $LiMnFe_2(PO_4)_3$ phases. The relative site stability found theoretically is in agreement with the experimental results that give the A(1) site as predominantly occupied by the sodium ions in $NaMnFe_2(PO_4)_3$. As the $LiMnFe_2(PO_4)_3$ could not be synthesized in this study, one cannot directly compare the experimental results to the theoretical ones performed on $LiMnFe_2(PO_4)_3$, but the trend is in agreement as A(1)′ is the most occupied site in $Li_{0.75}Na_{0.25}MnFe_2(PO_4)_3$.

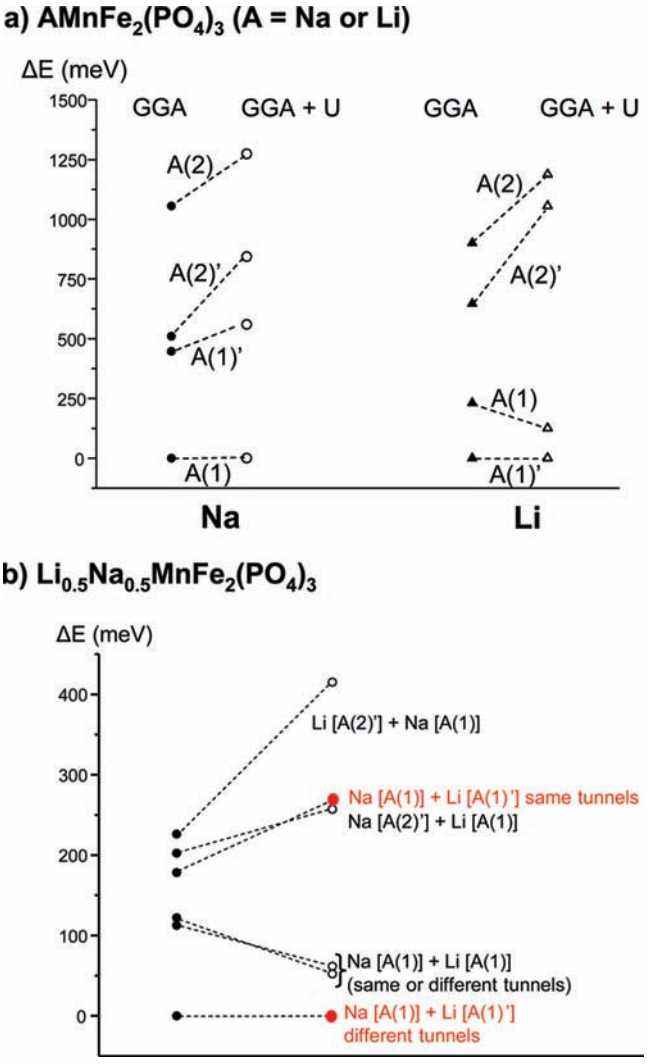

Figure 7. Investigation of the theoretical sodium and lithium sites stability in the alluaudite structure performed by GGA and GGA+U calculations. The energies of the structures are represented by their difference from the most stable structure, i.e., all Na in A(1) and expressed per $NaMnFe_2(PO_4)_3$ formula unit and all Li in A(1)′ and expressed per $LiMnFe_2(PO_4)_3$ formula unit.

(32) Antenucci, D.; Miehe, G.; Tarte, P.; Schmahl, W. W.; Fransolet, A.-M. *Eur. J. Mineral.* **1993**, *5*, 207–213.
(33) Hatert, F.; Antenucci, D.; Fransolet, A.-M.; Liégeois-Duyckaerts, M. *J. Solid State Chem.* **2002**, *163*, 194–201.
(34) Hidouri, M.; Lajmi, B.; Wattiaux, A.; Fournés, L.; Darriet, J.; Amara, M. B. *J. Solid State Chem.* **2004**, *177*, 55–60.
(35) Hatert, F.; Long, G. J.; Hautot, D.; Fransolet, A.-M.; Delwiche, J.; Hubin-Franskin, M. J.; Grandjean, F. *Phys. Chem. Miner.* **2004**, *31*, 487–506.
(36) Hatert, F. *Acta Crystallogr., Sect. C* **2006**, *C62*, i1–i2.
(37) Hermann, R. P.; Hatert, F.; Fransolet, A.-M.; Long, G. J.; Grandjean, F. *Solid State Sci.* **2002**, *4*, 507–513.
(38) Hatert, F. *Mineral Petrol.* **2004**, *81*, 205–217.
(39) Hatert, F. *J. Solid State Chem.* **2008**, *181*, 1258–1272.
(40) Abderrahim, A.; Ménétrier, M.; Croguennec, L.; Suard, E.; Delmas, C. *J. Mater. Chem.* **2002**, *12*, 2971–2978.

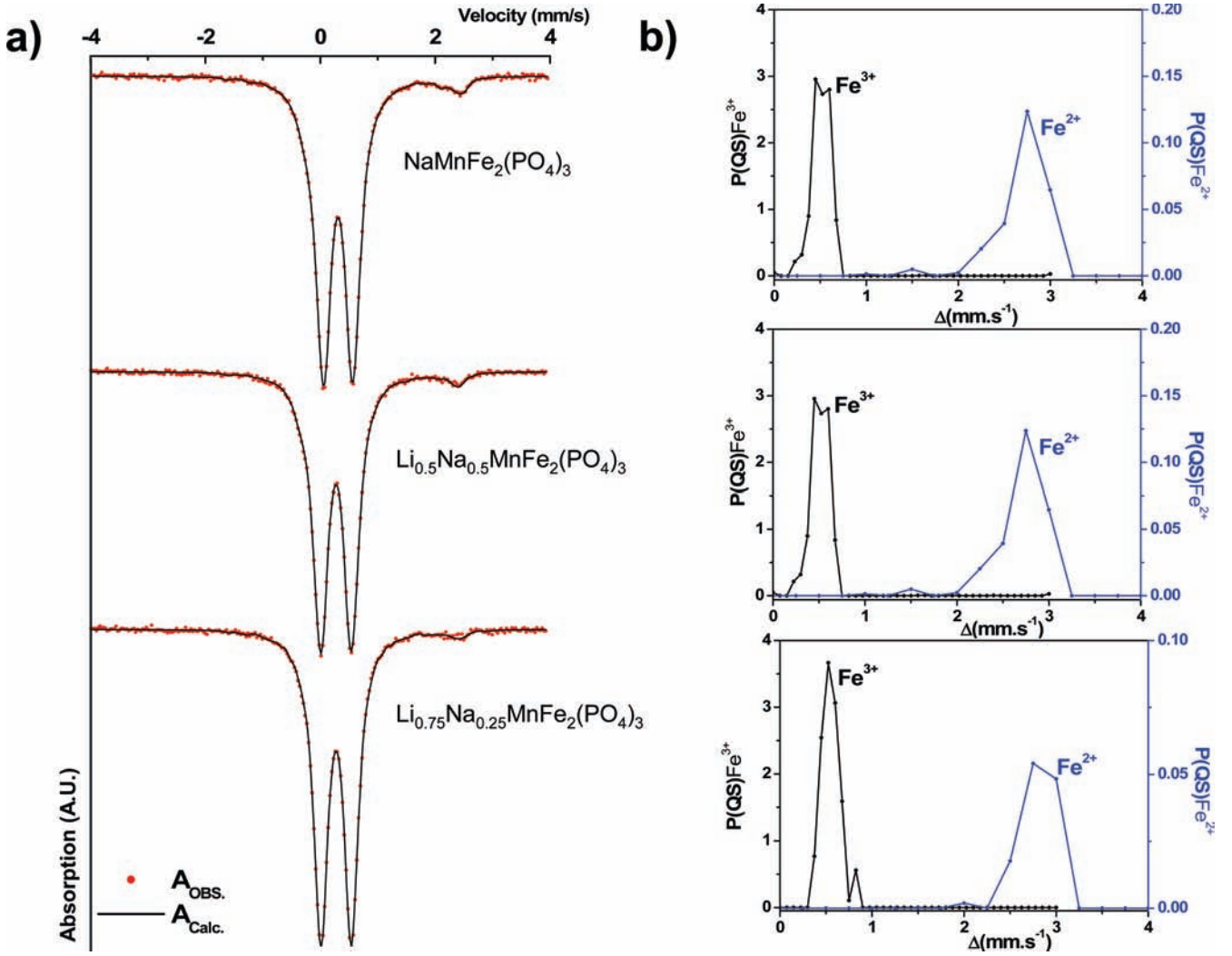

Figure 8. (a) Mössbauer experimental and fitted spectra of $NaMnFe_2(PO_4)_3$, $Li_{0.5}Na_{0.5}MnFe_2(PO_4)_3$, and $Li_{0.75}Na_{0.25}MnFe_2(PO_4)_3$. The corresponding fitted parameters are collected in Table 5. (b) The associated quadrupolar splittings distributions.

We also considered, by GGA and GGA+U methods, phases with the $Li_{0.5}Na_{0.5}MnFe_2(PO_4)_3$ composition, with the Li^+ and Na^+ ions located in different sites. The energy of the most stable configuration is used as the reference energy in Figure 7b, and the relative energies of some other cases are also reported. The most stable configuration is obtained for Na^+ and Li^+ located in the most stable sites previously identified individually for the $AMnFe_2(PO_4)_3$ (A = Na or Li) phases: Na in A(1) and Li in A(1)′. However, such a configuration was found to be the most stable, only if the Na^+ and Li^+ ions do not share the same tunnel (one tunnel 1 per unit cell contains only Na^+ ions, whereas the other tunnel 1 contains only Li^+ ions). If Li^+ and Na^+ ions were placed respectively in A(1)′ and A(1) sites in the same tunnels, alternatively, along the *c* direction, the $Li_{0.5}Na_{0.5}MnFe_2(PO_4)_3$ phase is much less stable (Figure 7b). This is explained by the fact that the occupation of adjacent A(1) and A(1)′ sites leads to a strongly repulsive interaction as it involves a very short Na−Li distance (experimentally, 1.6 Å). This configuration is even less stable than the one built with Na^+ and Li^+ ions both located in the A(1) sites ($d_{A(1)-A(1)}$ = 3.2 Å) of the same tunnels, but alternatively in the *c* direction. The energy loss to place Li^+ ions in the A(1) site that is not intrinsically the most stable one for Li^+ is compensated by a reduction of the repulsive electrostatic energy through an increase of the Na^+-Li^+ distance. Similar effects were considered in the $T^{\#}2-Li_XCoO_2$ phases to explain the occupation of the two different available Li sites.[41] Other configurations for $Li_{0.5}Na_{0.5}MnFe_2(PO_4)_3$, with an occupancy of sites in tunnel 2, did not lead to more stable phases.

These results are in agreement with the experimental ones that gave the A(1)′ site as the predominant one observed for Li in $Li_{0.75}Na_{0.25}MnFe_2(PO_4)_3$. Indeed, as

Table 5. Mössbauer Spectral Parameters for $Li_yNa_{1-y}MnFe_2(PO_4)_3$ (with y = 0, 0.5, and 0.75) Recorded at 293 K

	δ (mm/s)	Δ (mm/s)	Γ (mm/s)	%	site
$NaMnFe_2(PO_4)_3$[22]	0.434	0.58	0.25	93	Fe^{3+} [Oh]
	1.22	2.60	0.25	7	Fe^{2+} [Oh]
$Li_{0.5}Na_{0.5}MnFe_2(PO_4)_3$	0.430	0.60	0.25	94	Fe^{3+} [Oh]
	1.21	2.69	0.25	6	Fe^{2+} [Oh]
$Li_{0.75}Na_{0.25}MnFe_2(PO_4)_3$	0.431	0.58	0.25	96	Fe^{3+} [Oh]
	1.20	2.75	0.25	4	Fe^{2+} [Oh]

(41) Carlier, D.; Van der Ven, A.; Delmas, C.; Ceder, G. *Chem. Mater.* **2003**, *15*, 2651–2660.

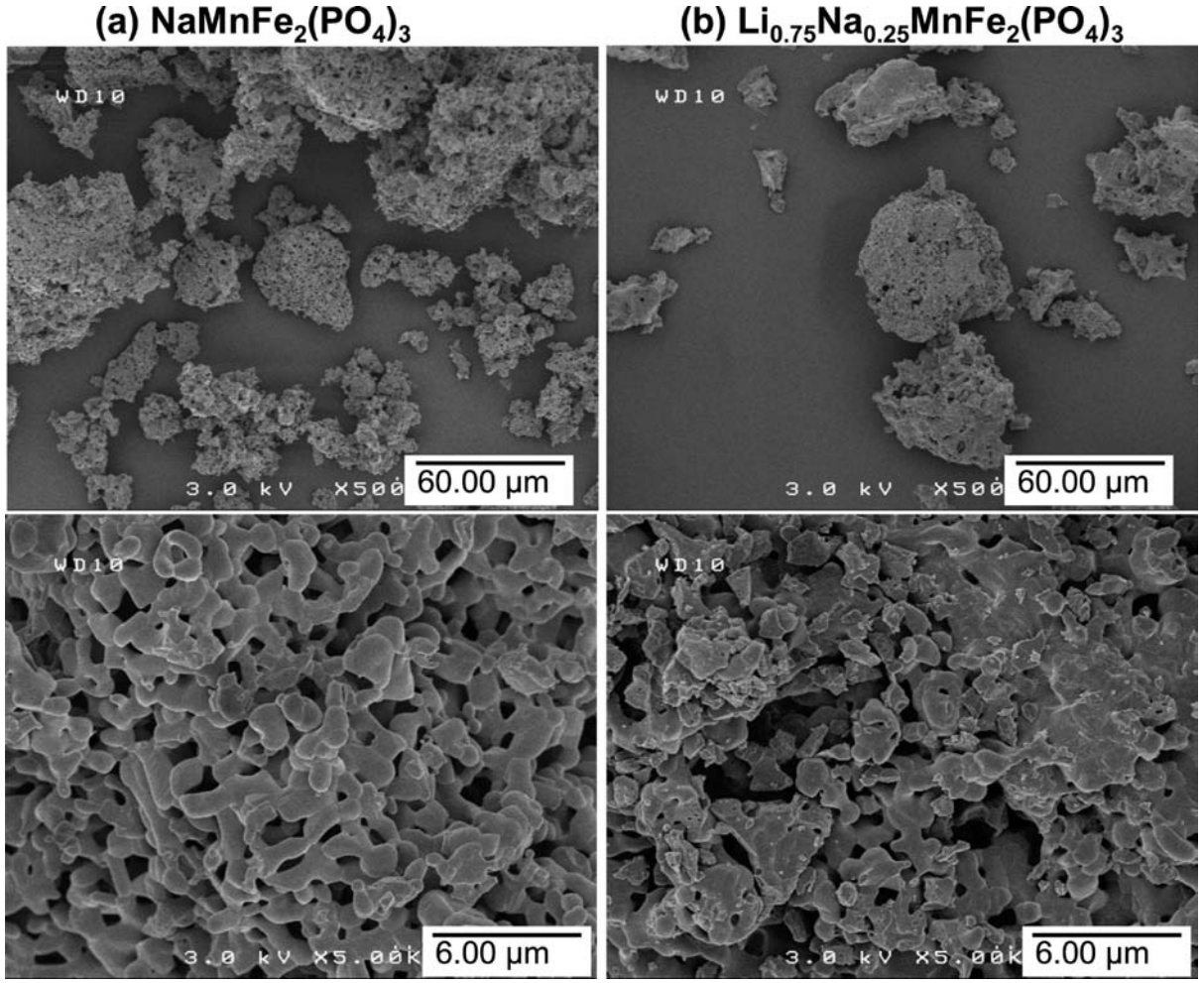

Figure 9. SEM micrographs showing the morphology and particle size of $NaMnFe_2(PO_4)_3$ (a) and $Li_{0.75}Na_{0.25}MnFe_2(PO_4)_3$ (b) powders.

almost no sodium ions are present in tunnel 1 (only 0.08, see Table 2) in this phase, the lithium ions occupy their most stable position, A(1)′. In $Li_{0.5}Na_{0.5}MnFe_2(PO_4)_3$, however, the A(1) site was found to be the predominant one (Table 2). In that case, 0.29 Na^+ ions are present in tunnel 1 in the A(1) sites, which destabilized the adjacent and next adjacent Li^+ A(1)′ sites (until there was a vacancy). This, therefore, results in a highest occupation of the A(1) sites for the lithium ions (0.29 Li^+ in A(1) and 0.21 Li^+ in A(1)′). Li^+ ions located in the A(1)′ sites would, therefore, be surrounded only by other Li^+ ions in A(1)′ (as second neighbors) or by vacancies (as first or even second neighbors).

The presence of Na^+ ions in A(2)′ with an amount that remains approximately constant (between 0.17 and 0.21 Na^+ ions) is not yet understood but appears to be independent of the Fe/Mn site ratio as the three $Li_yNa_{1-y}MnFe_2(PO_4)_3$ (y = 0, 0.5, 0.75) phases exhibit very different exchanged Fe/Mn amounts.

Fe/Mn Site Exchange. In $NaMnFe_2(PO_4)_3$, we observed an Fe/Mn site exchange between the M(1) and M(2) sites, which had been also observed for other Na−Mn−Fe[42] compounds. On the basis of Mössbauer spectroscopy and the bond valence sum method, we showed that the site exchange was associated with a change in the oxidation state of iron and manganese ions. In this study, Mössbauer spectroscopy was also used in order to check for the iron oxidation states in these lithium substituted phases that also exhibit a Mn/Fe site exchange, as revealed by neutron diffraction. Figure 8a shows the spectra recorded for $Li_{0.5}Na_{0.5}MnFe_2(PO_4)_3$ and $Li_{0.75}Na_{0.25}MnFe_2(PO_4)_3$. The corresponding spectrum of $NaMnFe_2(PO_4)_3$ is given for comparison. The general shape of the Mössbauer spectra indicates that they should be fitted with, at least, two doublets, one with a small isomer shift and a small quadrupole splitting assigned to Fe^{3+} ions and another with a large isomer shift and a large quadrupole splitting assigned to Fe^{2+} ions. A first conventional fit performed using two Lorentzian quadrupole doublets leads to large line width values, which suggests the existence of a distribution of quadrupolar splittings and therefore a distribution of local iron environments. The Mössbauer spectra were then further fitted considering two distributions of quadrupolar splittings (Figure 8b) with a constant value of the ^{57}Fe isotope line width (Γ = 0.25 mm/s) and the isomer shift fixed at the value determined in the first fit. The resulting Mössbauer spectra are represented in Figure 8a, and their corresponding parameters are listed in Table 5. The signal exhibiting a small isomer shift ($\delta \sim 0.43$ mm/s) and a small quadrupole splitting ($\Delta \sim 0.58$ mm/s) is attributed to trivalent iron Fe(III) ions

(42) Hatert, F.; Hermann, R. P.; Long, G. J.; Fransolet, A. M.; Grandjean, F. *Am. Mineral.* **2003**, *88*, 211–222.

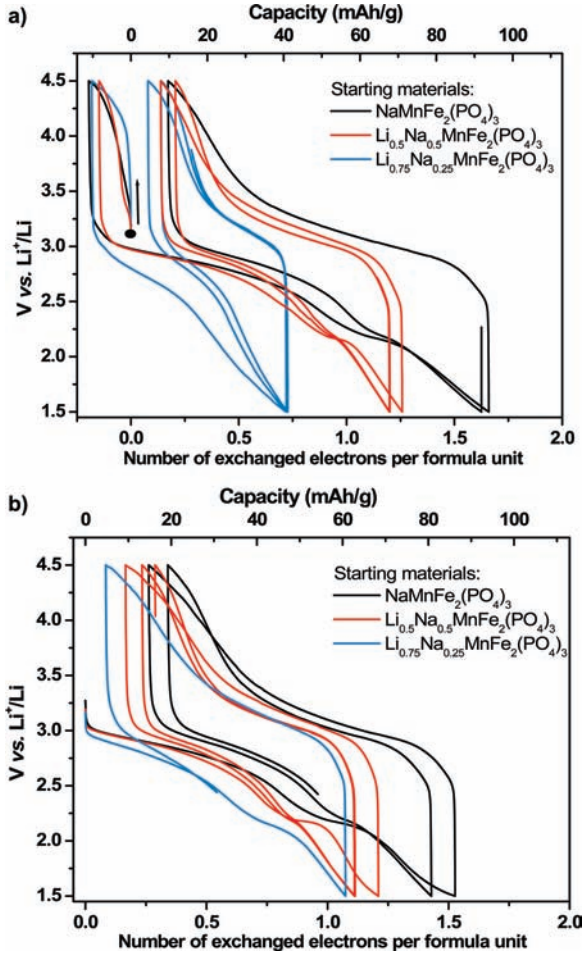

Figure 10. (a) Cycling curves recorded for a $Li//Li_yNa_{1-y}MnFe_2(PO_4)_3$ (with $y = 0$, 0.5, and 0.75) cell starting with a charge of the cell (C/50). (b) Cycling curves recorded for a $Li//Li_yNa_{1-y}MnFe_2(PO_4)_3$ (with $y = 0$, 0.5, and 0.75) cell starting with a discharge of the cell (C/50).

with a high-spin configuration and located in octahedral environments, as expected from the structure (M(2) site). The other signal, which exhibits a large isomer shift ($\delta \sim 1.21$ mm/s) and a large quadrupole splitting ($\Delta \sim 2.7$ mm/s), was attributed to high-spin Fe(II) ions located in the octahedral site. The amount of Fe^{2+} ions deduced from these Mössbauer measurements ranges from 7 to 4 atom % of the total Fe amount, and it decreases with increasing lithium content in the structure.

The amounts of Fe^{2+} ions deduced from Mössbauer spectroscopy (0.14 for $NaMnFe_2(PO_4)_3$,[22] ~0.12 for $Li_{0.5}Na_{0.5}MnFe_2(PO_4)_3$, and ~0.08 for $Li_{0.75}Na_{0.25}MnFe_2(PO_4)_3$) are on the same order of magnitude as that of the Fe ions found in the M(1) site due to the Mn/Fe site exchange evidenced by our neutron diffraction data analysis (0.13 for $NaMnFe_2(PO_4)_3$,[21] ~0.08 for $Li_{0.5}Na_{0.5}MnFe_2(PO_4)_3$, and ~0.04 for $Li_{0.75}Na_{0.25}MnFe_2(PO_4)_3$). We therefore assigned the Fe^{2+} Mössbauer signal to Fe^{2+} ions located in the M(1) octahedral sites. The substitution of Li^+ ions by Na^+ does not involve a strong modification of the local MO_6 geometry but leads to a decrease of the amount of Fe^{2+} ions seen by Mössbauer spectroscopy and therefore to a decrease of the Mn/Fe site exchange. The good quality of the X-ray and neutron refinements shown by the small difference and small reliability factors together with the results of Mössbauer spectroscopy suggests

Table 6. Theoretical Average Voltages Calculated to Remove 1 mol of Li^+ Ions or 1 mol of Na^+ Ions per $AMnFe_2(PO_4)_3$ Formula Unit in a Lithium Cell, Calculated with the GGA+U Method for Alkaline Ions Located in A(1), A(1)′, or A(2)′ sites

site	voltage Li vs Li^+/Li (V)	voltage Na vs Li^+/Li (V)
A(1)	4.78	5.05
A(1)′	4.90	
A(2)′		4.20

the adequacy of the proposed structural models to describe the structure of the two alluaudite compounds $Li_{0.5}Na_{0.5}MnFe_2(PO_4)_3$ and $Li_{0.75}Na_{0.25}MnFe_2(PO_4)_3$ that are rewritten, respectively: $(Li_{0.29})_{A(1)}(Li_{0.21})_{A(1)'}(Na_{0.29})_{A(1)}(Na_{0.21})_{A(2)'}(Mn^{II}_{0.92}Fe^{II}_{0.08})_{M(1)}(Fe^{III}_{1.92}Mn^{III}_{0.08})_{M(2)}(PO_4)_3$ and $(Li_{0.31})_{A(1)}(Li_{0.44})_{A(1)'}(Na_{0.08})_{A(1)}(Na_{0.17})_{A(2)'}(Mn^{II}_{0.96}Fe^{II}_{0.04})_{M(1)}(Fe^{III}_{1.96}Mn^{III}_{0.04})_{M(2)}(PO_4)_3$. The cell parameter evolution does not follow Vegards's law as sodium is substituted by lithium, since the sites occupied by the alkaline ions and the Fe/Mn site exchange magnitude both differ from one sample to the other.

Electrochemical Properties. The sol−gel synthesis applied to the preparation of $Li_{0.5}Na_{0.5}MnFe_2(PO_4)_3$ and $Li_{0.75}Na_{0.25}MnFe_2(PO_4)_3$ leads to the same morphology as $NaMnFe_2(PO_4)_3$ powder (see micrographs in Figure 9), i.e., aggregates ranging between 10 and 60 μm in diameter with spongy characteristics consisting of 1−3 μm primary particles. $Li_{0.5}Na_{0.5}MnFe_2(PO_4)_3$ and $Li_{0.75}Na_{0.25}MnFe_2(PO_4)_3$ were then studied as positive electrodes in lithium batteries. Figure 10 shows the galvanostatic cycling curves obtained between 1.5 and 4.5 V vs Li^+/Li for the two materials starting either by a charge (Figure 10a) or by a discharge (Figure 10b). For comparison, the cycling curve of $NaMnFe_2(PO_4)_3$ is also given.

During the first charge (Figure 10a), a similar amount of alkaline ions was removed for the three $Li_yNa_{1-y}MnFe_2(PO_4)_3$ materials with a pretty similar shape of the $V = f(x)$ curve and similar amounts of deintercalated ions. The small voltage step observed around 3.5 V for the $Li_{0.5}Na_{0.5}MnFe_2(PO_4)_3$ and $NaMnFe_2(PO_4)_3$ materials as positive electrodes is due to the oxidation of the small amount of Fe^{2+} ions and the Mn^{2+} ions present in these phases ($Li_{0.75}Na_{0.25}MnFe_2(PO_4)_3$ presented much fewer Fe^{2+} ions). The Fe^{2+} ion oxidation during the first charge was confirmed by Mössbauer spectroscopy. In order to get an idea of the average voltages expected to remove Na^+ ions or Li^+ ions from the alluaudite structure, we performed GGA+U calculations on hypothetical $MnFe_2(PO_4)_3$ and $AMnFe_2(PO_4)_3$ phases as end members with A = Li or Na. All Li^+ ions were placed successively in A(1) and A(1)′ sites and all Na^+ ions, in A(1) and A(2)′ sites. The GGA+U method was preferred over GGA, as it was shown to better reproduce the experimental voltages for other phosphate phases.[29] The energy difference between the $AMn^{II}Fe^{III}_2(PO_4)_3$ phases and the fully deintercalated one, $Mn^{III}Fe^{III}_2(PO_4)_3$, leads, in comparison to the energy of metallic Na or metallic Li, to the expected average voltages. A further shift of 0.3 V was performed to express the average voltage obtained to remove Na^+ ions relative to the Li^+/Li redox couple. Note that the calculations lead to a deintercalated $MnFe_2(PO_4)_3$ phase that exhibits only high spin Fe^{3+} and Mn^{3+} ions, indicating that the alkaline ion removal is associated with the oxidation of the Mn^{2+} ion to Mn^{3+}. The calculated average voltages are gathered in Table 6.

From these calculations, the Na^+ ions in A(2)′ sites (in tunnel 2) are the ones that should be deintercalated first, as they exhibit the smallest deintercalation voltage (4.2 V vs Li^+/Li). The deintercalation of the Li^+ ions in A(1) and A(1)′ (tunnel 1) sites should occur at a higher potential (4.78 and 4.90 V vs Li^+/Li) and seems not to occur in our potential window (up to 4.5 V). The Na^+ ions in A(1)′ sites are the most stable ones and would require an even higher voltage (5.05 V vs Li^+/Li) to be deintercalated. We therefore believe that in the three alluaudite phases considered, only the Na^+ ions in A(2)′ sites are deintercalated from the tunnels during the first charge up to 4.5 V vs Li^+/Li. Since the three materials exhibit a similar amount of Na^+ ions in these sites (0.19 in $NaMnFe_2(PO_4)_3$, 0.15 in $Li_{0.5}Na_{0.5}MnFe_2(PO_4)_3$, and 0.18 in $Li_{0.75}Na_{0.25}MnFe_2(PO_4)_3$), we observed roughly a similar deintercalated amount up to 4.5 V (Figure 10a).

After the first charge, the following discharge curves indicate that 0.7, 1.3, and 1.7 Li^+ ions per formula unit can be intercalated, respectively, in $Li_{0.75}Na_{0.25}MnFe_2(PO_4)_3$, $Li_{0.5}Na_{0.5}MnFe_2(PO_4)_3$, and $NaMnFe_2(PO_4)_3$. $NaMnFe_2(PO_4)_3$ exhibits the highest capacity: 96 mAh/g during the first discharge that follows the first charge. However, during the second charge, only 1.4 alkaline ions (Li^+ and/or Na^+) could be removed from $NaMnFe_2(PO_4)_3$ and, as expected, even less from $Li_{0.75}Na_{0.25}MnFe_2(PO_4)_3$ and $Li_{0.5}Na_{0.5}MnFe_2(PO_4)_3$. During the discharge, a voltage step is observed around 2.2 V for all materials that is not observed during the following charge. The voltage step diminishes upon further discharge cycles, indicating that there is a change in the alkaline ions distribution within the framework.

Figure 10b gives the cycling curves obtained for the three $Li_yNa_{1-y}MnFe_2(PO_4)_3$ materials used as positive electrodes in the lithium cell, starting with a discharge. The shape of the discharge and the amount of final intercalated lithium ions are similar to those observed in Figure 10a, as the batteries were first charged. This indicates that the removal of Na^+ ions in A(2)′ sites that is believed to occur during the first charge does not interfere strongly with the lithium intercalation process and does not improve the capacities reached after a few cycles.

Moreover, whatever the amount of lithium ions in the initial cathode material, the alluaudite structure can host a similar total amount of lithium ions in the structure: around 1.7 Li^+ ions at the end of the first discharge down to 1.5 V vs Li^+/Li, in total for the three phases. Therefore, lithium-free $NaMnFe_2(PO_4)_3$ exhibits the highest capacity: 96 mAh/g during the first cycle starting by a charge (Figure 10a), 85 mAh/g during the first discharge (Figure 10b), and about 74 mAh/g as reversible capacity.

Conclusion

The $Li_{0.5}Na_{0.5}MnFe_2(PO_4)_3$ and $Li_{0.75}Na_{0.25}MnFe_2(PO_4)_3$ alluaudite structures were investigated by Rietveld refinement of the X-ray and neutron diffraction data, which allows us to accurately locate the alkaline ions in the two tunnels of the structure, with occupation factors rather in agreement with our *ab initio* calculations of the site stabilities. Even if the alluaudite structure seems to be favorable to alkaline diffusion, $Li_{0.5}Na_{0.5}MnFe_2(PO_4)_3$ and $Li_{0.75}Na_{0.25}MnFe_2(PO_4)_3$ in lithium cells exhibit lower capacities compared to the nonlithiated compound $NaMnFe_2(PO_4)_3$.

Acknowledgment. The authors wish to thank ILL for the neutron diffraction experiment and especially Emmanuelle Suard, M3PEC, for calculation facilities; Cathy Denage, Philippe Dagault, and Laetitia Etienne for their technical assistance; and Stanislas Pechev for fruitful discussions.